

GT2006/90466

## COMPRESSOR BLADE OPTIMIZATION USING A CONTINUOUS ADJOINT FORMULATION

Dimitrios I. Papadimitriou \*

Laboratory of Thermal Turbomachines,  
 School of Mechanical Engineering,  
 National Technical University of Athens,  
 Athens, P.O. Box 64069, 15710, Greece  
 email: dpapadim@mail.ntua.gr

Kyriakos C. Giannakoglou †

Laboratory of Thermal Turbomachines,  
 School of Mechanical Engineering,  
 National Technical University of Athens,  
 Athens, P.O. Box 64069, 15710, Greece  
 email: kgianna@central.ntua.gr

### ABSTRACT

In this paper, a constrained optimization algorithm is formulated and utilized to improve the aerodynamic performance of a 3D peripheral compressor blade cascade. The cascade efficiency is measured in terms of entropy generation along the developed flowfield, which defines the field objective functional to be minimized. Its gradient with respect to the design variables, which are the coordinates of the Non-Uniform Rational B-Spline (NURBS) control points defining the blade, is computed through a continuous adjoint formulation of the Navier-Stokes equations based on the aforementioned functional. The steepest descent algorithm is used to locate the optimal set of design variables, i.e. the optimal blade shape. In addition to the well-known advantages of the adjoint method, the current formulation has even less CPU cost for the gradient computation as it leads to gradient expression which is free of field variations in geometrical quantities (such as derivatives of interior grid node coordinates with respect to the design variables); the computation of the latter would be costly since it requires remeshing anew the computational domain for each bifurcated design variable. The geometrical constraints, which depend solely on the blade parameterization, are handled by a quadratic penalty method by introducing additional Lagrange multipliers.

### NOMENCLATURE

$\vec{b}$	Vector of design variables
$e$	Energy per unit mass
$E$	Total energy per unit volume, $E = \rho e + \frac{1}{2}\rho u_i^2$
$\vec{f}_i^{inv}$	Inviscid flux array
$\vec{f}_i^{vis}$	Viscous flux array
$k$	Heat transfer coefficient
$\dot{m}$	Mass flow rate
$n_i$	Normal to the surface, unit vector component
$p$	Pressure
$q_i$	Thermal flux, $q_i = k \frac{\partial T}{\partial x_i}$
$s$	Specific entropy
$S_i$	Inlet Surface
$S_o$	Outlet Surface
$S_w$	Wall Surface
$t$	Time
$t_i$	Blade thickness
$T$	Temperature
$u_i$	Velocity components
$\vec{U}$	Vector of conservative variables
$\vec{V}$	Velocity vector
$x_i$	Cartesian coordinates
$\delta_{ij}$	Kronecker symbols
$\eta$	Steepest descent step size
$\mu$	Effective viscosity
$\vec{\Psi}$	Vector of adjoint variables
$\rho$	Density

\* PhD Student, National Technical University of Athens.

† Associate Professor, National Technical University of Athens.

$\tau_{ij}$  Viscous stress  
 $\Omega$  Volume

## INTRODUCTION

Analysis tools for numerically predicting flow fields in single or multiple turbomachinery rows have reached a trustworthy level. Based on these tools, numerous algorithms for the design of optimal blade shapes have been developed. The role of the analysis tools in optimization methods is to evaluate the performance of candidate blade geometries, associating with them an objective functional value. It is readily understood that randomized search algorithms are computationally demanding when dealing with complex 3D flows. Thus, smart search algorithms of either stochastic [1] or deterministic nature [2] have been proposed instead; their hybridization [3] is also possible. This paper deals exclusively with deterministic optimization methods which rely on the adjoint method for the computation of gradients.

Control theory [2,4–6] has proved to perfectly support aerodynamic shape design–optimization methods. The properly parameterized blade shape to be optimized “controls” the fluid flow within the blade row passage and determines its performance by means of a user–defined objective functional. The so–called adjoint method computes the gradient of the functional with respect to the design variables and a descent algorithm guides the search towards the optimal solution.

The present paper focuses on the aerodynamic optimization of a 3D peripheral compressor cascade; the optimal blade shape which, for the prescribed flow conditions and under certain geometrical constraints, gives minimum viscous losses is sought. The geometrical constraints concern the minimum allowed thickness of the blade; no other structural constraints or constraints related to flow turning are imposed. The performance of the peripheral cascade is measured in terms of entropy generation through the blade passage. Thus, the objective functional is defined as the difference in mass–averaged entropy between the inlet to the flow domain and its outlet. It is, then, transformed to a field integral in terms of velocity gradients; replacing entropy by terms involving temperature and velocity gradients was first proposed by Denton [7–9], as a means to account for profile losses in 2D turbomachinery cascades. The aforementioned theoretical framework is further exploited to set up a new continuous adjoint formulation [10] for the optimization of turbomachinery cascades, with certain advantages as described below. Our major concern is to derive objective function gradient expressions which are free of field terms. This is achieved by carefully treating terms which depend on the variation of flow and geometrical quantities’ gradients and simplifies the calculations by avoiding computing the variation of each internal grid node coordinate with respect to the design variables. The latter would otherwise be costly as it requires as many calls to the grid generation software as the number of design variables.

The geometrical constraint handling is taken into account through the Lagrange multiplier penalty method [11]. The gradients of the constraint functions are computed and used during the optimization procedure, finally leading to feasible solutions. The Spalart–Allmaras model, particularly adapted to compressible flows, is used for the calculation of the turbulent viscosity coefficient. Variations in turbulent viscosity are omitted.

## FLOW EQUATIONS AND OBJECTIVE FUNCTIONAL

Using the Einstein convention for repeated indices, the Navier–Stokes equations for the turbulent flow of a perfect gas are written as

$$\frac{\partial \vec{U}}{\partial t} + \frac{\partial \vec{f}_i^{inv}}{\partial x_i} - \frac{\partial \vec{f}_i^{vis}}{\partial x_i} = \vec{0} \quad (1)$$

where

$$\vec{U} = \begin{bmatrix} \rho \\ \rho \vec{V} \\ E \end{bmatrix}, \quad \vec{f}_i^{inv} = \begin{bmatrix} \rho u_i \\ \rho u_i \vec{V} + p \delta_i \\ u_i (E + p) \end{bmatrix}, \quad \vec{f}_i^{vis} = \begin{bmatrix} 0 \\ \tau_i \\ u_j \tau_{ij} + q_i \end{bmatrix} \quad (2)$$

and

$$\tau_{ij} = \mu \left( \frac{\partial u_i}{\partial x_j} + \frac{\partial u_j}{\partial x_i} \right) + \lambda \delta_{ij} \frac{\partial u_k}{\partial x_k}, \quad \lambda = -\frac{2}{3} \mu \quad (3)$$

In the present application, the objective functional to be minimized is defined as the difference in mass averaged entropy  $s$  between the inlet  $S_i$  to and outlet  $S_o$  from the flow domain,

$$F = \int_{S_o} s d\dot{m} - \int_{S_i} s d\dot{m} = \int_{S_{i,o}} \rho V_n s dS = \int_S \rho V_n s dS \quad (4)$$

Using Gauss’ divergence theorem and the continuity equation, Eq. (4) is transformed to a field integral over the flow domain  $\Omega$ , as follows

$$F = \int_{\Omega} \rho u_i \frac{\partial s}{\partial x_i} d\Omega \quad (5)$$

Eq. (5) is further expressed in terms of temperature and velocity gradients as

$$F = \int_{\Omega} \frac{1}{T} \tau_{ij} \frac{\partial u_i}{\partial x_j} d\Omega \quad (6)$$

The integrand in Eq. (6) was proposed in [7–9] for 2D boundary layers to express the total rate of entropy creation, viz. the viscous shear work being converted to heat at temperature  $T$ . Although profile losses are associated with boundary layers,  $F$  is defined over the whole computational domain  $\Omega$ , since the viscous stresses and velocity gradients outside the boundary layer are comparatively negligible. By minimizing the profile losses, total pressure losses are expected to reduce, too.

### ADJOINT EQUATIONS, BOUNDARY CONDITIONS AND SENSITIVITY DERIVATIVES

The integral of the variation of the flow equations, multiplied by the adjoint variables  $\vec{\Psi}$  over  $\Omega$ , is added to the variation of  $F$  yielding thus the variation of the augmented objective functional  $F_{aug}$ , namely

$$\delta F_{aug} = \delta F + \int_{\Omega} \vec{\Psi}^T \delta \left( \frac{\partial \vec{f}_i^{inv}}{\partial x_i} - \frac{\partial \vec{f}_i^{vis}}{\partial x_i} \right) d\Omega \quad (7)$$

In order to formulate the adjoint problem, Gauss' divergence theorem is applied to reduce the order of flow variable variations. In Eq. (7), the variation in the gradient should be transformed to the gradient of a variation. This can be done by considering that any flow variable  $\Phi$  depends on both grid coordinates and design variables. By expressing (a) the variation in  $\Phi$  with respect to the design variables, (b) the variation in the gradient of  $\Phi$  and (c) the gradient of the variation in  $\Phi$ , it can be shown [12] that

$$\delta \left( \frac{\partial \Phi}{\partial x_i} \right) = \frac{\partial(\delta \Phi)}{\partial x_i} - \frac{\partial \Phi}{\partial x_k} \frac{\partial(\delta x_k)}{\partial x_i} \quad (8)$$

Eq. (8) expresses the variation in any spatial derivative of  $\Phi$  in terms of the spatial derivative of  $\delta \Phi$  and the scalar product of the gradient of  $\Phi$  and the same spatial derivative of the variation in the position vector; the latter accounts for variations in grid node coordinates due to the variation in design variables  $\vec{b}$  controlling the geometry. Using Eq. 8, the variation in gradients is transformed to gradients of variations and Gauss' divergence theorem can be employed. The latter is used to develop terms including gradients of both flow and geometrical variations (applied once for the inviscid terms and twice for the viscous terms) and leads to the final expression for the augmented functional variation [10, 12], namely

$$\begin{aligned} \delta F_{aug} = & \int_{S_w} R_{ij} \frac{\partial u_j}{\partial x_k} n_i \delta x_k dS + \int_{S_w} \frac{1}{T} R \delta x_i n_i dS + \int_{S_w} \frac{\mu}{T} R_{ij} n_j \delta u_i dS - \\ & \int_{\Omega} \left( \delta \vec{U}^T - \frac{\partial \vec{U}^T}{\partial x_k} \delta x_k \right) \left( A_i^T \frac{\partial \vec{\Psi}}{\partial x_i} - M^{-T} \vec{K} - M^{-T} \vec{L} \right) + \\ & \int_{\Omega} \vec{\Psi}^T \frac{\partial}{\partial x_k} \left( \frac{\partial \vec{f}_i^{inv}}{\partial x_i} - \frac{\partial \vec{f}_i^{vis}}{\partial x_i} \right) \delta x_k d\Omega - \\ & \int_{S_w} \frac{\partial \vec{U}^T}{\partial x_k} A_n^T \vec{\Psi} \delta x_k dS + \int_{S_w} \Psi_{i+1} n_i \delta p dS + \\ & \int_{S_w} (\Psi_{i+1} p - \vec{\Psi}^T \vec{f}_i) \delta(n_i dS) + \int_{S_{i,o}} \delta \vec{U}^T (A_n^T \vec{\Psi}) dS + \\ & \int_{S_w} \delta u_i \left[ \mu \left( \frac{\partial \Psi_{j+1}}{\partial x_i} + u_j \frac{\partial \Psi_5}{\partial x_i} + \frac{\partial \Psi_{i+1}}{\partial x_j} + u_i \frac{\partial \Psi_5}{\partial x_j} \right) + \right. \\ & \left. \lambda \delta_{ij} \left( \frac{\partial \Psi_{k+1}}{\partial x_k} + u_k \frac{\partial \Psi_5}{\partial x_k} \right) - \Psi_5 \tau_{ij} \right] n_j dS + \\ & \int_{S_w} \delta T \left( k \frac{\partial \Psi_5}{\partial x_i} n_i \right) dS - \int_{S_w} \Psi_5 \delta(q_j n_j dS) + \\ & \int_{S_w} \Psi_5 q_j \delta(n_j dS) - \int_{S_w} \frac{\Psi_{i+1}}{n_i} [\delta \tau_{ij} n_i n_j + \tau_{ij} \delta(n_i n_j)] dS + \\ & \int_{S_w} \frac{\Psi_{i+1}}{n_i} \tau_{ij} \delta(n_i n_j) dS - \int_{S_w} u_i \Psi_5 \delta \tau_{ij} n_j dS - \\ & \int_{S_w} \frac{\partial u_i}{\partial x_l} \left[ \mu \left( \frac{\partial \Psi_{j+1}}{\partial x_i} + u_j \frac{\partial \Psi_5}{\partial x_i} + \frac{\partial \Psi_{i+1}}{\partial x_j} + u_i \frac{\partial \Psi_5}{\partial x_j} \right) \right. \\ & \left. \lambda \delta_{ij} \left( \frac{\partial \Psi_{k+1}}{\partial x_k} + u_k \frac{\partial \Psi_5}{\partial x_k} \right) \right] \delta x_l n_j dS + \\ & \int_{S_w} \frac{\partial T}{\partial x_k} \left( k \frac{\partial \Psi_5}{\partial x_i} \right) \delta x_k n_i dS - \int_{S_w} \vec{\Psi}^T \frac{\partial \vec{f}_i^{vis}}{\partial x_k} \delta x_k n_i dS \quad (9) \end{aligned}$$

The elimination of all field terms which depend on the variations in  $\vec{U}$  gives rise to the field adjoint equations:

$$\frac{\partial \vec{\Psi}}{\partial t} - A_i^T \frac{\partial \vec{\Psi}}{\partial x_i} - M^{-T} \vec{K} - M^{-T} \vec{L} = \vec{0} \quad (10)$$

where

$$\begin{aligned} K_1 = & \frac{T}{\rho} \frac{\partial}{\partial x_i} \left( k \frac{\partial \Psi_5}{\partial x_i} \right) \\ K_{i+1} = & \frac{\partial}{\partial x_j} \left[ \mu \left( \frac{\partial \Psi_{j+1}}{\partial x_i} + u_j \frac{\partial \Psi_5}{\partial x_i} + \frac{\partial \Psi_{i+1}}{\partial x_j} + u_i \frac{\partial \Psi_5}{\partial x_j} \right) + \right. \end{aligned}$$

$$K_5 = \frac{T}{p} \frac{\partial}{\partial x_i} \left( k \frac{\partial \Psi_5}{\partial x_i} \right) - \lambda \delta_{ij} \left( \frac{\partial \Psi_{k+1}}{\partial x_k} + u_k \frac{\partial \Psi_5}{\partial x_k} \right) - \tau_{ij} \frac{\partial \Psi_5}{\partial x_j}$$

and

$$\begin{aligned} L_1 &= \frac{1}{T^2} R \frac{\partial T}{\partial \rho} \\ L_{i+1} &= \frac{1}{T^2} R \frac{\partial T}{\partial u_i} \frac{\partial}{\partial x_j} \left( \frac{\mu}{T} R_{ij} \right) \quad , \quad i = 1, 2, 3 \\ L_5 &= \frac{1}{T^2} R \frac{\partial T}{\partial E} \end{aligned}$$

$M$  is the Jacobian matrix of the transformation from the conservative to the non-conservative flow variables.

The surface integrals defined over the inlet, outlet and solid walls, which also depend on flow variations, are eliminated too, giving rise to the boundary conditions for  $\vec{\Psi}$ . At the inlet and outlet, viscous terms can be neglected, so  $\delta \vec{U}^T (A_n^T \vec{\Psi}) = 0$ . Over the wall surfaces,  $\Psi_2 = \Psi_3 = \Psi_4 = 0$ , while either homogeneous Dirichlet or Neumann condition can be imposed for  $\Psi_5$ , depending on the corresponding temperature condition. Here, adiabatic wall conditions were used, so  $\frac{\partial \Psi_5}{\partial n} = 0$ .

Once the field adjoint equations and their boundary conditions have been satisfied, the remaining terms in Eq. (9) read

$$\begin{aligned} \delta F_{aug} &= - \int_{S_w} \left( \vec{\Psi}^T \vec{f}_i \right) \delta(n_i dS) - \int_{S_w} \frac{\partial \vec{U}^T}{\partial x_k} (A_i^T n_i) \vec{\Psi} \delta x_k dS + \\ &\int_{S_w} \left( \vec{\Psi}^T \frac{\partial \vec{f}_{vi}}{\partial x_k} \right) \delta x_k n_i dS + \int_{S_w} \Psi_5 q_j \delta(n_j dS) - \\ &\int_{S_w} \frac{\partial u_i}{\partial x_l} \left[ \mu \left( \frac{\partial \Psi_{j+1}}{\partial x_i} + u_j \frac{\partial \Psi_5}{\partial x_i} + \frac{\partial \Psi_{i+1}}{\partial x_j} + u_i \frac{\partial \Psi_5}{\partial x_j} \right) + \right. \\ &\quad \left. \lambda \delta_{ij} \left( \frac{\partial \Psi_{k+1}}{\partial x_k} + u_k \frac{\partial \Psi_5}{\partial x_k} \right) \right] \delta x_l n_j dS - \\ &\int_{S_w} R_{ij} \frac{\partial u_j}{\partial x_k} n_i \delta x_k dS + \int_{S_w} \frac{1}{T} R \delta x_i n_i dS \end{aligned} \quad (11)$$

where

$$R = \tau_{ij} \frac{\partial u_i}{\partial x_j} \quad , \quad R_{ij} = 2(1 + \delta_{ij}) \frac{\partial u_i}{\partial x_j} + 2(1 - \delta_{ij}) \frac{\partial u_j}{\partial x_i} - \frac{4}{3} \delta_{ij} \frac{\partial u_k}{\partial x_k}$$

Given a shape parameterization in terms of  $\vec{b}$ , Eq. (11) is used to compute the gradient of  $F_{aug}$  with respect to the design

variables. This gradient supports the search of the optimal blade shape, which is carried out using the steepest descent algorithm, controlled by a step size  $\eta$  (see next section). From Eq. (11), it can be deduced that, although  $F$  was a field integral, its gradient expression is free of field terms, depending solely on integrals defined on the parameterized wall surfaces.

## CONSTRAINT HANDLING

In order to prevent the optimization procedure from converging to “non-acceptable” blade geometries,  $n$  geometrical constraints are imposed. These constraints control the minimum allowed thickness at certain points along the cascade blade. So, the blade thickness  $t_i$  at a number of preselected points should always exceed predefined minimum allowed values  $t_i^{min}$ . Each constraint is cast in the form of an inequality  $C_i = t_i^{min} - t_i \leq 0$ .

These inequality constraints are handled using Lagrange multipliers and penalty coefficients [11]. The inequality constrained optimization problem

$$\begin{aligned} \min F_{aug} \\ \text{s.t. } C_i \leq 0 \quad , \quad i = 1, n \end{aligned} \quad (12)$$

is first transformed to an equivalent equality constrained problem

$$\begin{aligned} \min F_{aug} \\ \text{s.t. } C_i + z_i^2 = 0 \quad , \quad i = 1, n \end{aligned} \quad (13)$$

by introducing the variables  $z_i$ . Introducing additional Lagrange multipliers  $\lambda_i$  and the penalty coefficient  $w$ , the constrained problem (13) becomes equivalent to the following unconstrained one

$$\min F_{c,aug} = F_{aug} + \sum_{i=1,n} \lambda_i (C_i + z_i^2) + \sum_{i=1,n} \frac{w}{2} (C_i + z_i^2)^2 \quad (14)$$

The optimal value for  $z_i$  is  $z_i^2 = \max[0, -(\frac{\lambda_i}{w} + C_i)]$  and the update formula for the Lagrange multipliers is  $\lambda_i^{k+1} = \lambda_i^k + w^k (C_i^k + z_i^2)$ , where  $k$  is the optimization cycle counter.

Theoretically [11], the minimization of  $F_{c,aug}$  converges to the optimal solution for continuously increasing values of the penalty coefficient  $w$ . Additionally, numerical experiments recommend that  $\eta$  should decrease from cycle to cycle.

The gradient of the second and third term on the r.h.s. of Eq. (14) needs to be computed too and the gradient of  $F_{c,aug}$  with respect to  $\vec{b}$  drives the steepest descent algorithm towards convergence, according to the update rule

$$\vec{b}^{k+1} = \vec{b}^k - \eta \left( \frac{\delta F_{c,aug}}{\delta \vec{b}} \right)^k \quad (15)$$

## CONSTRAINED OPTIMIZATION ALGORITHM

This section presents an outline of the iterative algorithm used to solve the constrained optimization problem. For the sake of brevity, we introduce five operators which govern the evaluation of the performance of any blade cascade with respect to the previously stated objective function, the constraint handling as well as the solution of the adjoint equations. So: (a)  $BLADE(\vec{b})$  builds the blade shape using the actual set of values of  $\vec{b}$  through the NURBS theory [13], (b)  $GRID(BLADE(\vec{b}))$  generates the computational grid in the cascade passage, (c)  $THICKNESS(BLADE(\vec{b}))$  computes thicknesses  $t_i$ , (d)  $FLOW(GRID(BLADE(\vec{b})))$  solves the flow equations, Eqs. (1) and (e)  $ADJOINT(\vec{U}, GRID(BLADE(\vec{b})))$  solves the adjoint equations, Eqs. (10). The iterative algorithm is as follows:

**Step 0:** Starting values of the design variables  $\vec{b}^0$ , Lagrange multipliers  $\lambda_i^0$  and penalty coefficient  $w^0$  are set ( $k=0$ ).

**Step 1:** The blade shape is built ( $BLADE(\vec{b}^k)$ ), the necessary thicknesses are computed ( $THICKNESS(BLADE(\vec{b}^k))$ ) and the computational grid generated ( $GRID(BLADE(\vec{b}^k))$ ).

**Step 2:** The derivatives of geometrical quantities (such as unit normal vectors  $\vec{n}$ , finite areas  $dS$ ) with respect to  $\vec{b}$  are computed at each grid node over the blade surface, using finite-difference schemes. For this purpose, the non-costly  $BLADE(\vec{b}^k \pm \vec{\epsilon})$  operator, where  $\vec{\epsilon}$  is an infinitesimal increment per component of  $\vec{b}$ , is repeatedly applied.

**Step 3:** Derivatives  $\frac{dt_i}{d\vec{b}}$  of blade thicknesses with respect to  $\vec{b}$  and consequently  $\frac{dC_i}{d\vec{b}}$  are computed directly from the derivatives calculated in the previous step.

**Step 4:** The flow equations are solved for the given flow conditions using  $FLOW(GRID(BLADE(\vec{b}^k)))$  and  $\vec{U}^k$  is computed.

**Step 5:** The adjoint equations are solved using  $ADJOINT(\vec{U}^k, GRID(BLADE(\vec{b}^k)))$  and  $\vec{\Psi}^k$  is computed.

**Step 6:** The objective function gradient  $\frac{dF_{c,aug}}{d\vec{b}}$  is computed and the design variables  $\vec{b}^{k+1}$  are updated using the steepest descent formula, Eq. (15)

**Step 7:** The Lagrange multipliers  $\lambda^{k+1}$  and the penalty coefficient  $w^{k+1}$  are updated, as described in the previous section. Go to step 1, with  $k = k + 1$ .

## RESULTS–DISCUSSION

In this section, the previously described optimization algorithm is applied to the design of a 3D peripheral compressor cas-

cade where the objective is the minimization of entropy increase within the flow passage, at a single operating point. At this point, the isentropic exit Mach number is 0.5, the inlet flow is axial and the chord-based Reynolds number is  $5 \times 10^5$ .

The flow solver is a 3D Navier–Stokes equations solver for H-type structured grids based on a vertex-centered, finite-volume discretization. It uses an upwind formulation for the inviscid fluxes, employing Roe’s approximate Riemann solver [14] and variable extrapolation to account for second-order accuracy. The van Leer–van Albada limiter [15] is used to cope with inaccuracies owing to highly stretched grids. The Spalart–Allmaras, low-Reynolds turbulence model [16] is used.

The gradient of the objective functional is calculated using the continuous adjoint formulation described above. The adjoint PDEs are discretized using a Roe-type discretization scheme [17] and the same limiter is employed to overcome inaccuracies in the calculation of gradients.

The cascade is parameterized using 3D NURBS, separately for the blade pressure and suction sides. 13 control points are placed in the longitudinal direction and 5 in the radial one, thus resulting in a total of 65 control points per blade surface. Only the control points placed along the hub and tip are directly controlled by  $\vec{b}$ . The interior control points in the spanwise direction are placed by linearly interpolating the hub and tip ones. For the “primitive” control points (i.e. those comprising  $\vec{b}$ ), only their peripheral coordinates are free to vary. Thus, 28 free variables are to be optimized in total ( $\vec{b} \in R^{28}$ ).

The cascade is formed by 61 blades with a (spanwise constant) stagger angle of 27 deg. An H-type structured grid of  $191 \times 55 \times 71$  nodes is generated at step 1 of the repetitive algorithm by solving elliptic type equations with appropriate source terms.

The convergence of the optimization algorithm for the selected tuning parameters is obtained within 35 cycles. Fig. (1) shows the evolution of the objective function value during the cycles; it stands for the entropy generation (here, non-dimensionalized entropy, in conformity to the non-dimensionalization of the flow equations). From this figure, it is obvious that the entropy generation varies non-monotonically during the first 15 cycles, during which feasible and infeasible shapes are generated. This can be seen by examining Fig. (2). In the latter, the sum of values of the geometrical constraint function,  $\sum_{i=1,n} \max(C_i, 0)$ , is plotted in terms of cycles. During the first cycles, the frequent violation of the constraints is obvious. However, after the 15th cycle, all constraints are satisfied; some slight violations of constraints after the 15th cycle can practically be neglected.

The pressure coefficient distribution along the blade midspan, for both the starting and optimal blade are shown in Fig. (3). They correspond to the iso-Mach contours at midspan, plotted in Fig. (4). The total pressure loss coefficient in the cascade is reduced from  $\omega = 0.038$  to  $\omega = 0.033$ . Note that the

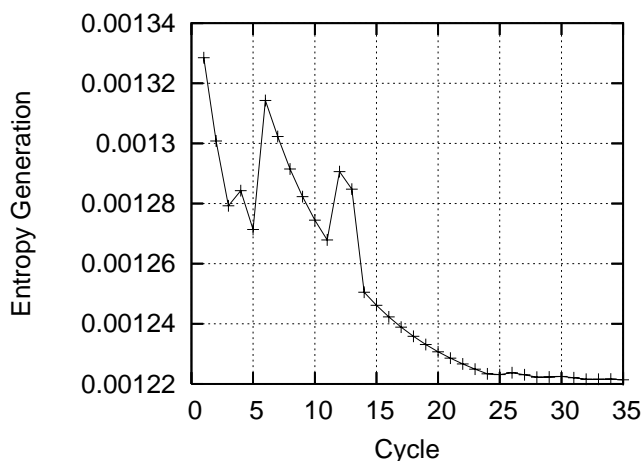


Figure 1. Convergence of entropy generation rate.

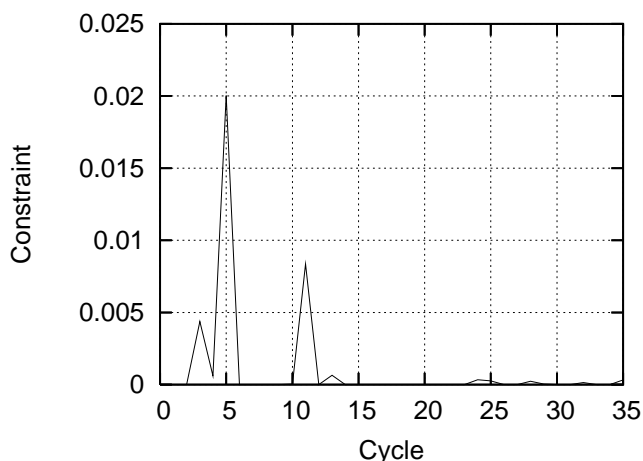


Figure 2. Sum of geometrical constraints,  $\sum_{i=1,n} \max(C_i, 0)$ , showing the violation of constraints in each cycle.

improvement is considerable (13%) due to the fact that the imposed constraints practically allowed a small reduction in the blade thickness. The 3D computational grid and the pressure distribution over a part of the peripheral cascade are illustrated in figs. (5) and (6).

The initial and optimal set of control points for the blade hub, Fig. (7), and tip, Fig. (8), are also shown. A 3D view of the initial and optimal control points is shown in Fig. (9). In Figs. (10) and (11), the blade airfoils at the hub and tip are illustrated. All these figures reveal the same tendency for the blade geometry and control points. The blade contour slope right after the leading edge becomes milder and the blade tends to become thinner; however any further reduction in the blade thickness is avoided due to the constraint imposition. If the geometrical constraints are not taken into account, the optimization algorithm

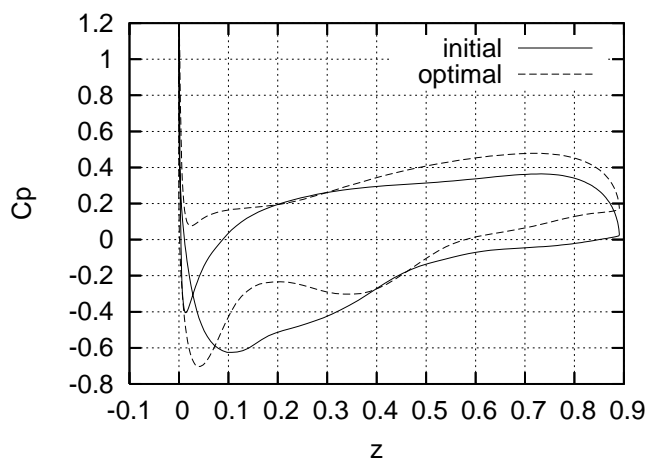


Figure 3. Pressure coefficient distribution for the initial and optimal blade at midspan.

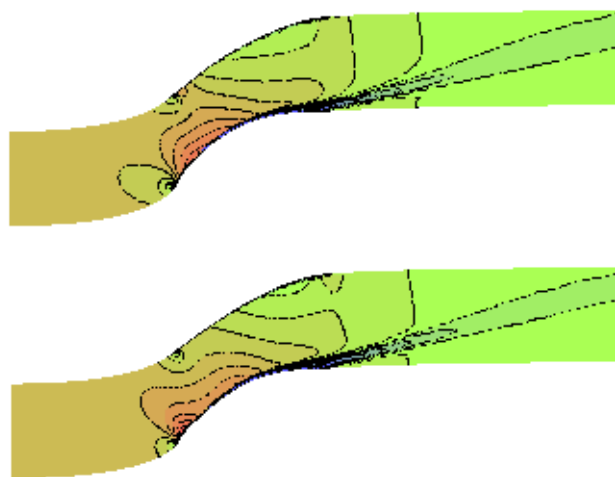


Figure 4. Mach number distribution for the initial (top) and the optimal (bottom) blade at midspan. Maximum Mach=0.95, increment=0.0475.

tends to continuously reduce the blade thickness. As expected, the reduction in thickness starts at the leading edge. Computational experiments showed that the objective functional reduces until the thickness of the blade becomes almost zero, resulting of course in an infeasible shape solution.

The convergence trend of the optimization algorithm and the physical meaning of the final solution is further clarified with Fig. (12). The derivatives of the objective functional  $F$  measuring the entropy generation with respect to the control points defining the suction side are positive for both hub and tip (14 first values); in contrast, the same derivatives for the pressure side control points are negative. Thus, generally, the blade tends to become thinner. By carefully examining the same figure, one

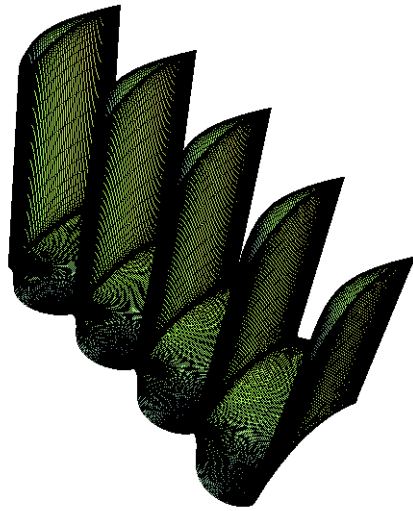


Figure 5. 3D computational grid over the blade and hub surfaces of the optimal peripheral cascade.

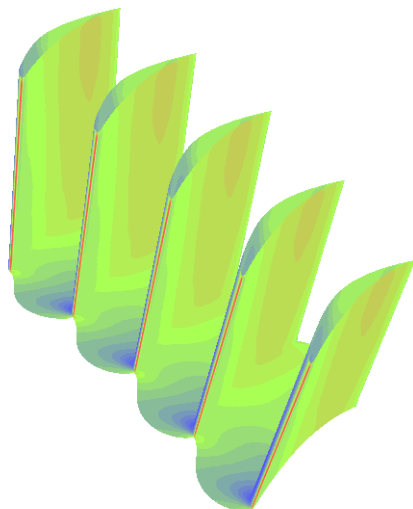


Figure 6. Mach number distribution over the blade and hub surfaces of the optimal peripheral cascade. Minimum  $P=1.4\text{bar}$ , maximum  $P=2.5\text{bar}$ , increment= $0.055\text{bar}$ .

might notice that the derivatives of the suction side control points near the leading edge have comparatively higher values. This leads to greater reduction of their values during the descent algorithm. When the blade becomes too thin in this region, the constraint gradient “reacts” on both suction and pressure sides. As a consequence, although the pressure side control points tend to approach the suction side ones (thus thinning the blade), the constraint forces them move in the opposite direction.

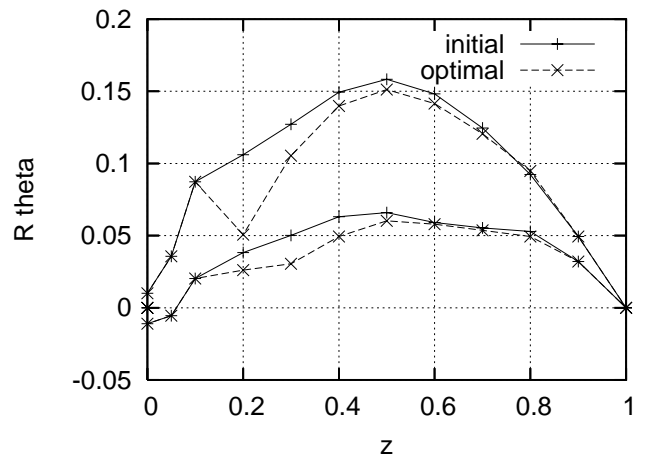


Figure 7. Initial and optimal control points for the blade hub.

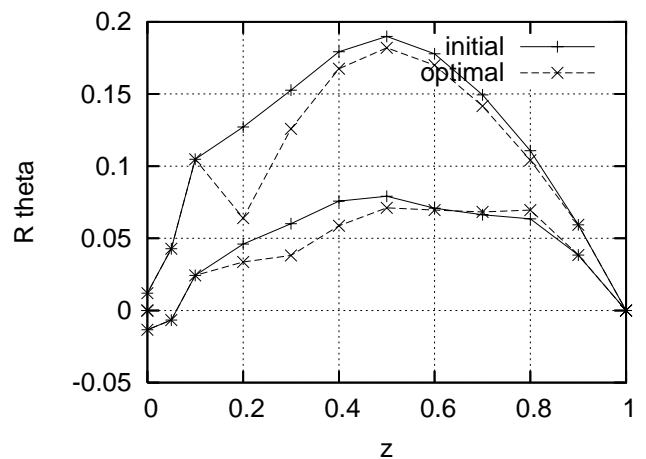


Figure 8. Initial and optimal control points for the blade tip.

## CONCLUSIONS

A new continuous adjoint formulation for the optimization of turbomachinery blades was presented. The objective functional was defined in terms of the entropy generation within the blade passage. By considering that this is mainly due to the profile losses, the objective functional took the form of a field integral expressed in terms of velocity gradients and temperature. The handling of terms expressing the variation of spatial gradients, as shown in detail in this paper, led to the objective function gradient which is free of field terms. Geometrical constraints are imposed using additional Lagrange multipliers and a penalty coefficient. The algorithm proved to be non-costly and the cost for the design of a peripheral compressor cascade was equivalent to approximately 70 flow solutions (35 solutions of the flow equations and an equal number of solutions of the adjoint equations, both considered to have almost the same computational

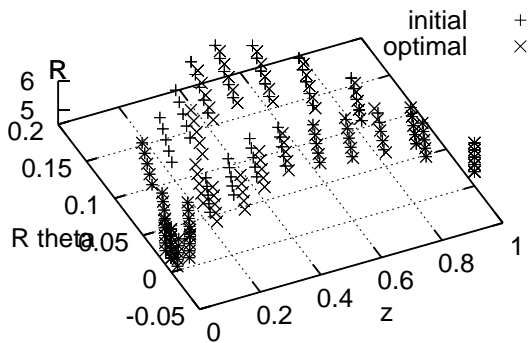


Figure 9. 3D view of the initial and optimal control points.

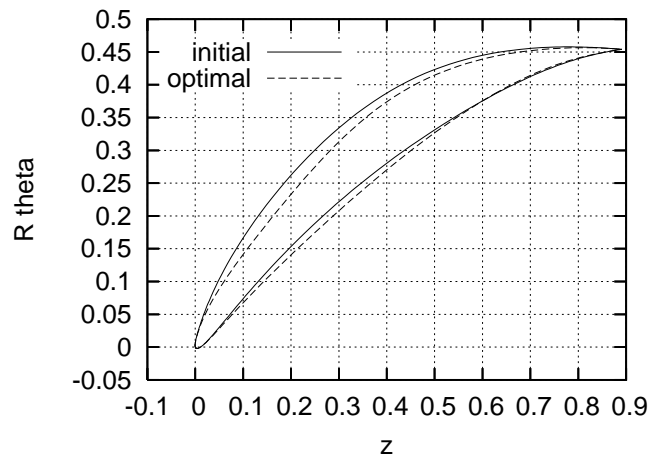


Figure 11. Initial and optimal blade contours at tip.

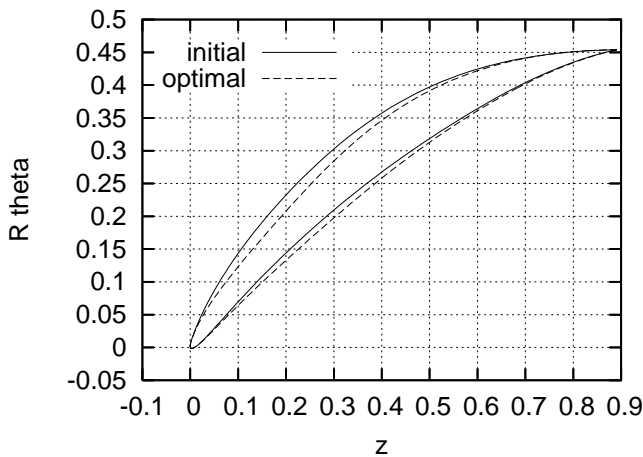


Figure 10. Initial and optimal blade contours at hub.

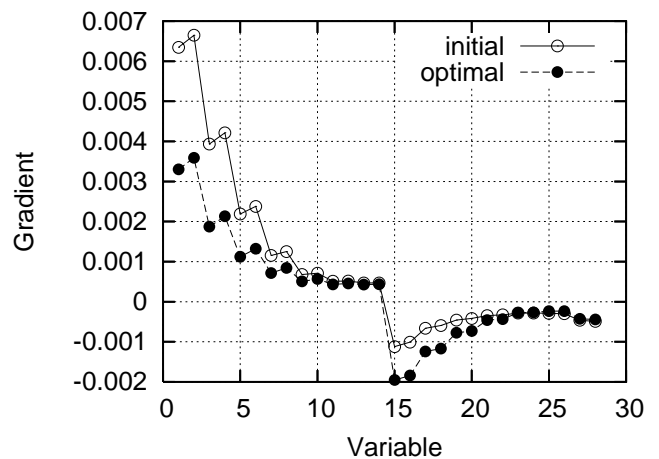


Figure 12. Objective functional gradient components corresponding to each one of the design variables. The first 14 variables parameterize the suction side. The remaining ones correspond to the pressure side. Note that the gradient of  $F_{aug}$  (instead of  $F_{c,aug}$ ) is plotted. According to Figs. (10) and (11), the optimal blade “moved” towards its pressure side so that the gradient components at pressure side nodes are higher than that of the initial blade.

cost). The proposed method overcomes repetitive grid generation at each cycle, which is the standard technique to compute derivatives of the coordinates of interior grid nodes with respect to the design variables.

## ACKNOWLEDGMENT

The project is co-funded by the European Social Fund (75%) and National Resources (25%) - Operational Program for Educational and Vocational Training (EPEAEK) and, particularly, the IRAKLITOS Program.

## REFERENCES

[1] K.C. Giannakoglou. Designing turbomachinery blades using evolutionary methods. ASME Paper 99-GT-181, 1999.

- [2] A. Jameson, N. Pierce, and L. Martinelli. Optimum aerodynamic design using the Navier-Stokes equations. AIAA Paper 94-4272-CP, 1994.
- [3] I.C. Kampolis, D.I. Papadimitriou, and K.C. Giannakoglou. Evolutionary optimization using a new radial basis function network and the adjoint formulation. *Journal of Inverse Problems in Engineering*, to appear, 2005.
- [4] A. Jameson. Aerodynamic design via control theory. *Journal of Scientific Computation*, 3:33–260, 1988.
- [5] A. Jameson. Optimum aerodynamic design using cfd and

- control theory. AIAA Paper 95-1729-CP, 1995.
- [6] M.B. Giles and N.A. Pierce. Adjoint equations in CFD: Duality, boundary conditions and solution behaviour. AIAA Paper 97-1850, 1997.
  - [7] J.D. Denton. Loss mechanisms in turbomachines. ASME Paper 93-GT-435, 1993.
  - [8] M.R.D. Davies, F.K. O'Donnell, and A.J. Niven. Turbine blade entropy generation rate, part i: The boundary layer defined. ASME Paper 2000-GT-265, 2000.
  - [9] F.K. O'Donnell and M.R.D. Davies. Turbine blade entropy generation rate, part ii: The measured loss. ASME Paper 2000-GT-266, 2000.
  - [10] D.I. Papadimitriou and K.C. Giannakoglou. A continuous adjoint method with objective function derivatives based on boundary integrals for inviscid and viscous flows. *Journal of Computers and Fluids*, to appear, 2006.
  - [11] D.P. Bertsekas. *Nonlinear Programming*. Athena Scientific, 2nd edition, 1999.
  - [12] D.I. Papadimitriou, A.S. Zymaris, and K.C. Giannakoglou. Discrete and continuous adjoint formulations for turbomachinery applications. EUROGEN 2005, Int. Conf. Proceedings, Munich, September 2005.
  - [13] L. Piegl and W. Tiller. *The NURBS Book*. Springer, 2nd edition, 1997.
  - [14] P. Roe. Approximate Riemann solvers, parameter vectors, and difference schemes. *Journal of Computational Physics*, 43:357–371, 1981.
  - [15] G.D. van Albada, B. van Leer, and W.W. Roberts. A comparative study of computational methods in cosmic gas dynamics. *Astron. Astrophys.*, 108:76–84, 1982.
  - [16] P.R. Spalart and S.R. Allmaras. A one-equation turbulence model for aerodynamic flows. *La Recherche Aerospaciale*, (1):5–21, 1994.
  - [17] W.K. Anderson and V. Venkatakrishnan. Aerodynamic design optimization on unstructured grids with a continuous adjoint formulation. *Computers and Fluids*, 28:443–480, 1999.